



New coating synthesis comprising CuO:NiO/C to obtain highly selective surface for enhancing solar energy absorption

Rasheed N. Abed¹ · Mustafa Abdalh² · Alaa A. Rashad² · Abas Hadawey³ · Emad Yousif²

Received: 1 October 2019 / Revised: 6 January 2020 / Accepted: 22 January 2020 /
Published online: 4 February 2020
© Springer-Verlag GmbH Germany, part of Springer Nature 2020

Abstract

A novel nano coating was synthesized by spin and casting methods to obtain high-performance selective surfaces to enhance solar energy absorption. Nanomaterials (CuO:NiO) and carbon (fly ash) were used to provide a cost-efficient coating with high absorption efficiency. The materials were prepared with different carbon doping content, and the coating of the nanocomposite film was deposited by these techniques on pre-cleaned copper and glass substrates. Energy dispersive X-ray analysis was used to determine the component element for carbon (fly ash), and its diameter was measured using scanning electron microscopy. The optical properties were investigated by UV spectrometry and reflectivity tests in a range of 250–1300 nm at room temperature. The absorbance coefficient, transmittance, reflectance, skin depth, optical density, optical energy gap and Urbach's parameters of the nanocomposite thin films were also determined. The data were analyzed and interpreted in terms of the theory of phonon-assisted direct electronic transitions. The E_g of the doped carbon was measured in different composition ratios of CuO:NiO ($A = 0.5:2.5$, $B = 1:2$, $C = 1.5:1.5$, $D = 2:1$, $E = 2.5:0.5$) wt.%, and fixed carbon content at 7 wt.%. The results of the doped samples revealed an energy gap value of 2.5–3.9 eV. When the ratio of the CuO content ranged from 0.5 to 2.5, composition B was found to have three regions in its figure that were dependent on the CuO content in the nanocomposite mixture. The optical band gap values were highly dependent on the CuO content in the nanocomposite films.

Keywords Nanocomposite · Nanomaterials · Optical properties · Energy gap · Urbach energy

✉ Rasheed N. Abed
rasheednema@eng.nahrainuniv.edu.iq; rasheednema@yahoo.com

Extended author information available on the last page of the article

Introduction

Nanocomposite compounds have recently become a focus of interest for many researchers as a result of the evolution of selective surface techniques for absorption of solar energy. They have shown potential for use in a number of optical devices operating in the UV–visible and near-infrared (NIR) ranges [1, 2]. Nanocomposite film coating in selective surfaces is dependent on the band gap and may be deemed more suitable for absorbing all ranges of the electromagnetic spectrum for solar energy [3, 4]. Moreover, thin film nanocomposites can be designed in accord with the maximum range of the visible spectrum and NIR, enabling the tailoring and adjustment of their physical features [5–7].

Thin film nanocomposites are semiconductors that can be used in coating, catalysis, and solar energy absorption, and are currently found in a number of significant technology applications. The behavior of thin films is further determined by their surface microstructure and interface morphology and the elemental composition of the chemical compounds, and their optical and electrical properties are dependent on the film thickness [6–8]. In addition, with regard to the optical features of nanocomposite thin films, the refractive index values are often lower than those of bulk materials, while the absorption coefficients are often higher than those of the same bulk materials. In this work, the nanocomposite utilizes the combined features of CuO and NiO, and is characterized by high absorption in the visible and near-IR regions. In addition, the composition of the materials in the nanocomposite can be tuned to achieve the best optical band gap [9–11]. No previous studies have investigated CuO:NiO nanocomposite for doping of carbon (fly ash) to obtain thin films, and the effects on their optical properties such as transmittance, reflectance, optical density, energy band gap, skin depth, and Urbach energy [12–16]. With regard to the properties of CuO and NiO with respect to carbon doping, nano copper oxide (CuO) has exceptional catalytic activity, as evidenced by its application in gas sensors, environmental catalysis, electrochemical cells, transistors, and solar cells. These properties differ strongly from the bulk phase. CuO is a p-type semiconductor with superconducting properties and demonstrates a narrow band gap (1.2 eV) for the bulk phase, but this band gap depends on the annealing temperature, and increased particle size will lead to an increase in band gap and absorption wavelength. [17–19]. The Cu foam doping of CuO/ZnO creates a huge surface area and heterojunction of the ZnO/CuO composite to boost the photo-catalytic performance, and thus is useful for application in the photodegradation of organic dyes [20, 21]. On the other hand, ZnO was doped by the Cu component not only inside the lattice but also covering its surface and giving it electrochemical properties for the solar cell with changed Cu content [22, 23]. CuO doping of tin oxide (SnO₂) with different content also exhibits effects on optical and electrical properties. Measurements show that an increase in CuO content leads to increased conductivity and transfer of charge carriers from n- to p-type [24, 25]. Moreover, the addition of CuO to NiO results in a significant increase in particle size and a decrease in surface area, which leads to an increase in the crystalline phase for the hybrid nano oxides. For

this mixture, the agglomeration size increases with increasing NiO in CuO and increased calcification temperature from 400 to 600 °C, with increased crystallite size of the particles [26, 27].

Therefore, nano NiO is a good example of a p-type semiconductor with a wide energy band gap (range 3.2–4.0 eV) [28]. When Cu doping of NiO is used, the obtained films will also be a p-type, which is deposited by spray pyrolysis. The resistance of these films decreases with an increase in Cu content, and the conductivity of the films depends on the prepared solution. The absorption coefficient for these films and their band gaps are dependent on the Cu composition for doping of NiO [29–32]. Nickel (Ni) is then used to dope CuO, and the thin film produced is synthesized by the sol–gel method to achieve magnetic properties. The magnetization of this film decreases with increased temperature and depends on the content of Ni in CuO, which will lead to a decrease in the magnetization in the lattice for the composite Ni:CuO [33, 34]. Further, a composite NiO:PVA was synthesized and its optical properties studied by examining the effect of NiO-doped PVA with various NiO content. The results demonstrated the effect of NiO on optical features for the PVA and showed a decrease in band gap for the PVA from 3.82 to 3.6 eV [35–37]. Similarly, nano Cu₂O was coated on multi-walled carbon nanotubes (MWCNTs) via a simple one-step reaction using Fehling's reagent, and demonstrated the ability to disperse Cu₂O on different surface substrates such as graphite and graphene [38–42]. Another strategy involves a polyaniline nanostructured composite with different percentages of carbon black. The nanocomposite was formed as a result of the alignment of molecules in the micelle. This system shows maximum electrical conductivity of about 1.38 S/cm, which is three times that of the original polyaniline with no additives [7]. These approaches can be utilized in applications such as optoelectronics, electromagnetic interference shielding, rechargeable batteries, sensors and electrochemical energy storage, photocatalysis and nano-electronics [43–47]

Therefore, the objective of the present work was to complete an assessment and analysis of the optical properties of thin films of CuO:NiO with doping of carbon to improve the physical properties of carbon. To the best of our knowledge, there is no study published to date on the optical properties of CuO:NiO/C. The objective of the present work was to prepare CuO:NiO/C thin films having different dopant concentrations by using solution spin casting. The absorbance of the films was recorded using UV–Vis spectroscopy, and measurements such as skin depth, optical density and Urbach energy were calculated to determine the best composition of the nanocomposite for use as a coating on a flat plate collector to absorb solar energy. This can be used in domestic heating applications, and offers the advantage of heating from the sun as a source of energy, which is available year round for countries around the world.

Experimental work

The nanocomposite was synthesized from the solution and deposited by spin and casting to obtain nanocomposite thin films on the Cu and glass substrates.

Preparation and characterization of the materials

Carbon (fly ash) obtained as a product of combustion was supplied by Midland Refineries Company (MRC)/Daura Refineries. The fly ash was sieved to remove all lingering particles. As shown in Fig. 1a, scanning electron microscopy (SEM) was used to measure the particle size of the fly ash, which was 29.62–93.22 μm , and demonstrated the morphology of the carbon (fly ash). Figure 1b shows the energy-dispersive spectroscopy (EDS) analysis of the carbon. EDS was performed using an Inspect S50 low-vacuum (3 nm at 30 kV SE) SEM to determine the purity of the carbon utilized in the nanocomposite thin film.

CuO and NiO were supplied by Changsha Easchem Company (Hunan, China), with particle size of 58.43 and 30.69 nm, respectively, and purity of 99.9%. Atomic force microscopy (AFM) was used to determine the particle size for the nanomaterial particles as shown in Fig. 2, which is the same particle size as that received from the Chinese company and confirmed that the particles were nanomaterials.

SEM for nanocomposite thin film

The surface morphology of the nanocomposite thin film is shown in Fig. 3 for different content of CuO:NiO with carbon (fly ash). A SEM image of the nanocomposite thin film showing the surface morphology is shown in Fig. 3a, and characterization by AFM is shown in Fig. 3b. These images reveal the porous structure of the nanocomposite thin film, which will enhance the absorbance of the solar energy radiation.

Figure 3a reveals that the nanocomposite dielectric thin film layer structure of CuO:NiO/C is a spectrally selective surface, with good properties of surface coating shape. The AFM image of the nanocomposite thin film in Fig. 3b shows a fine roughness of the surface, leading to high absorbance through the surface in the visible and IR region for the incident wavelength.

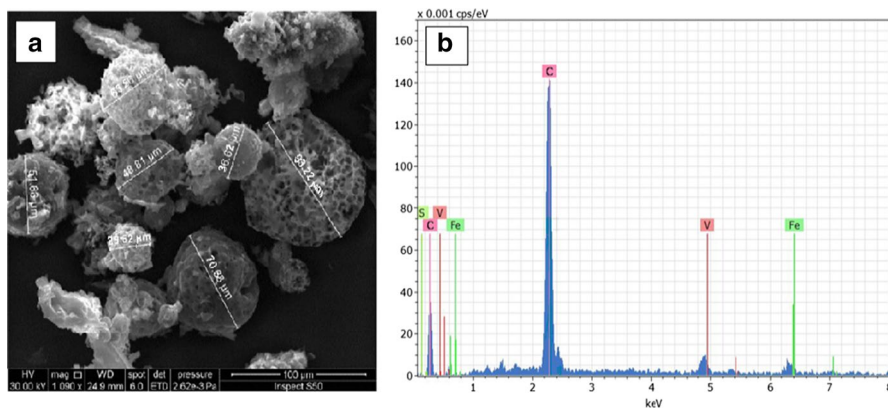


Fig. 1 EDS test for carbon (fly ash) by SEM

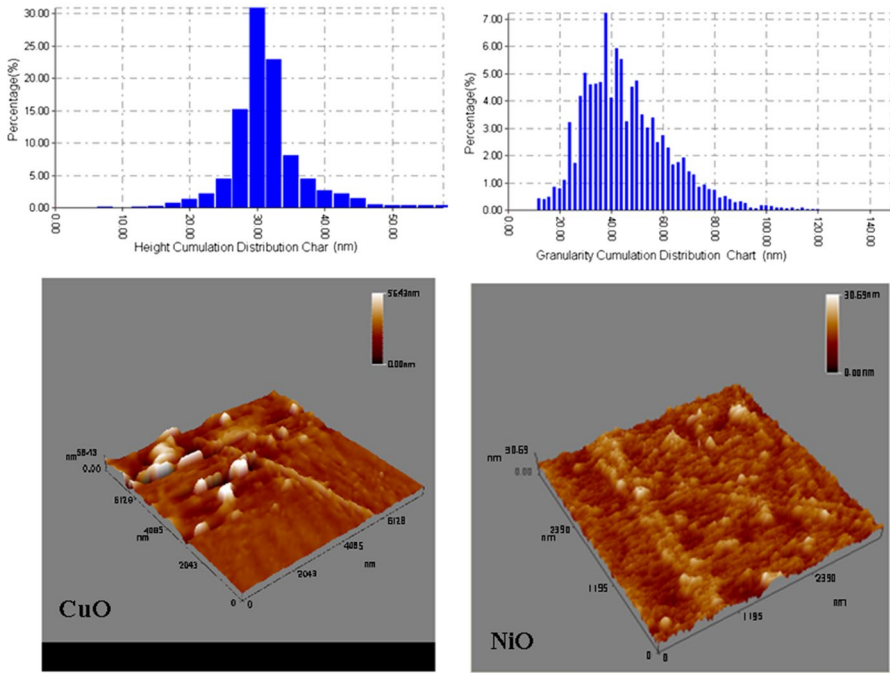


Fig. 2 AFM inspection for CuO and NiO nanomaterials

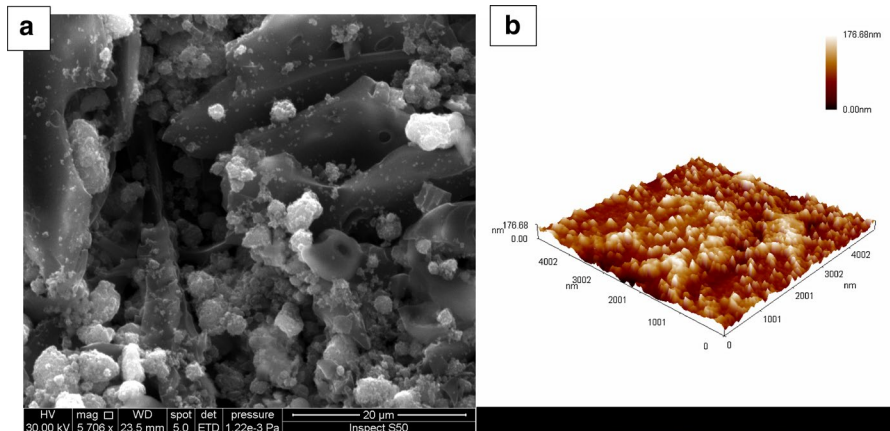


Fig. 3 a SEM and b AFM analysis for the CuO:NiO/C nanocomposite

XRD inspection of the nanocomposite

The crystal structure was characterized to examine the crystallite properties of the CuO:NiO/C nanocomposite thin film under the various precipitating measurements by utilizing the X-ray diffraction (XRD) patterns [radiation/wavelength: Cu

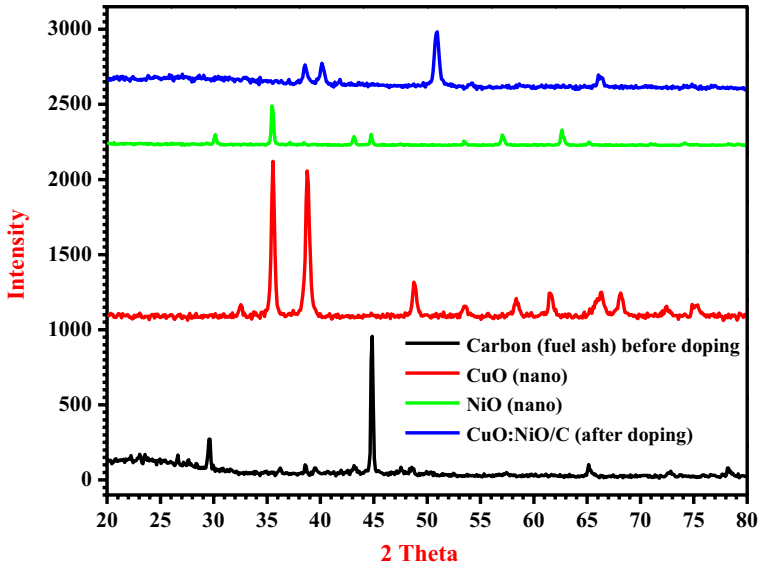


Fig. 4 XRD patterns for the CuO, NiO nano, carbon (fly ash), and the nanocomposite

Table 1 Values of the intensity with theta for CuO, NiO nano, carbon (fly ash) and CuO:NiO/C nanocomposite

Carbon (fly ash)		CuO		NiO		CuO:NiO/C	
2 Theta (θ°)	Intensity	2 Theta (θ°)	Intensity	2 Theta (θ°)	Intensity	2 Theta (θ°)	Intensity
29.6	271	32.5	156	30.2	71	38.6	186
44.9	956	35.6	1128	35.5	263	40.2	196
65.2	102	38.8	1085	43.2	59	51.0	406
72.6	46	48.8	323	44.8	74	66.1	118
78.2	80	53.5	161	53.5	30		
		58.4	215	57.0	69		
		61.5	249	62.7	103		
		66.3	254				
		68.05	237				
		72.1	133				
		74.1	175				

K- α 1.54056 Å (high-resolution)] and inspected in the 2θ range (20° – 80°) with a Cu-K α 1 target and a monochromator at (40 kV and 250 mA). Figure 4 shows the XRD patterns of the CuO, NiO nanomaterials, carbon (fly ash), and the nanocomposite film, with the intensities of all the compounds forming the composite. The X-ray diffraction of the nanocomposite thin film annealed at 300°C was produced, and the intensity peaks with the theta of XRD pattern were collected from Fig. 4, and the results are show in Table 1.

Synthesis of the nanocomposite

The starting materials of carbon (fly ash) powdered and nano CuO:NiO were weighed, and their mass ratios in appropriate proportions in stoichiometric quantities as determined by an electronic balance (5 digits) were used to obtain the desired composition. Carbon content fixed at 7% was added to high-purity CuO:NiO of varying composition ($A=0.5:2.5/7$, $B=1:2/7$, $C=1.5:1.5/7$, $D=2:1/7$, $E=2.5:0.5/7$) wt.% to obtain a homogeneous solution mixture. A stirrer was used for 2 h to stir the solid components with deionized water and molasses to ensure thorough mixing. The nanocomposite thin films were then synthesized. The solution was placed in a glass tube followed by vigorous mixing; the nanocomposite thin films were deposited on Cu and glass substrates with dimensions of $2.5 \times 5 \text{ cm}^2$, which had been thoroughly cleaned several times using a detergent solution, ethanol, and acetone to remove any grease on them, after which they were rinsed in deionized water and dried in an oven at $50 \text{ }^\circ\text{C}$ for 1 h. The nanocomposite samples were deposited on substrates by spin coating and casting, and dried in an oven at $80 \text{ }^\circ\text{C}$ to remove any residual solution in the samples. The thickness of the fabricated nanocomposite thin films was 300 nm.

Characterization

The prepared samples were analyzed using computerized diffuse reflectance spectroscopy (Avantes DH-S-BAL-2048 UV–Vis). Spectra were recorded in a wavelength range of 250–1300 nm in steps of 2 nm. Then, using the computerized Shimadzu UV-1650 PC UV–visible Spectrophotometer, the absorbance spectra were recorded in the wavelength range of 200–800 nm also in steps of 2 nm. All optical investigations were carried out at room temperature (300 K).

Results and discussion

Optical properties studies

Absorbance coefficient

The optical properties of materials depend on many variables such as the preparation method, surface morphology, and precursor conditions, according to their interaction with the environment. The investigation of the spectral coefficient of absorption for any semiconducting material provides additional information regarding the levels of electrons in the high-energy region of the optical absorption spectrum, while the low-energy region of the spectrum corresponds to the vibrations of atoms [48, 49]. Different applications are dependent on the optical absorption spectrum of the

CuO:NiO/C nanocomposite, and the absorption coefficient can be determined from the measurement of absorbance values with the wavelength and computed from the Beer–Lambert law [50, 51]:

$$\ln \frac{I}{I_0} = e^{-\alpha t}, \alpha = 2.303 * \frac{A}{t} \quad (1)$$

where α is the absorbance coefficient (cm^{-1}), A is the absorbance value, and t is the thickness (cm).

The optical absorbance coefficient of the CuO:NiO/C nanocomposite thin films ($0.05:2.5 \leq x \leq 2.5:0.05$ at wt.%) is dependent on the wavelength, as shown in Fig. 5. The results in the figure show that the absorption coefficient (α) decreases with the increase in wavelength for all samples of the CuO:NiO nanocomposite until a certain wavelength (about ~ 800 nm). The thin film samples were dependent on the film coating, and after that the coefficient (α) for the wavelength was nearly invariable.

In each composition, the absorption edge was determined by extrapolating the decreased fraction of the absorption coefficient curve to intersect the wavelength line at a specific point. The point of intersection indicates the optical band edge amount. It was observed that the intersection points are located in the UV–visible zone for all nanocomposite thin films, and the absorption edge is shown in Fig. 6. The results of the composition of the nanocomposites on the start of the curve change with the wavelength. It was observed that with an increase in the CuO ratio, the absorption edge was increased across wavelengths. In the nanocomposite thin films, the absorption edge values of composition $A=326$ nm, $B=338$ nm, $C=328$ nm, $D=332$ nm, and $E=336$ nm respectively. It is clear from Fig. 6 that the highest value of the absorption edge is

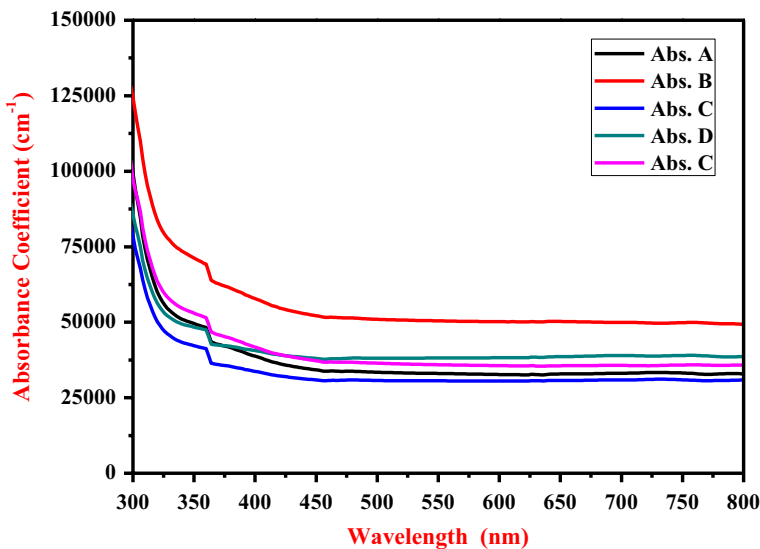


Fig. 5 Absorption coefficient variation with the wavelength for the nanocomposite

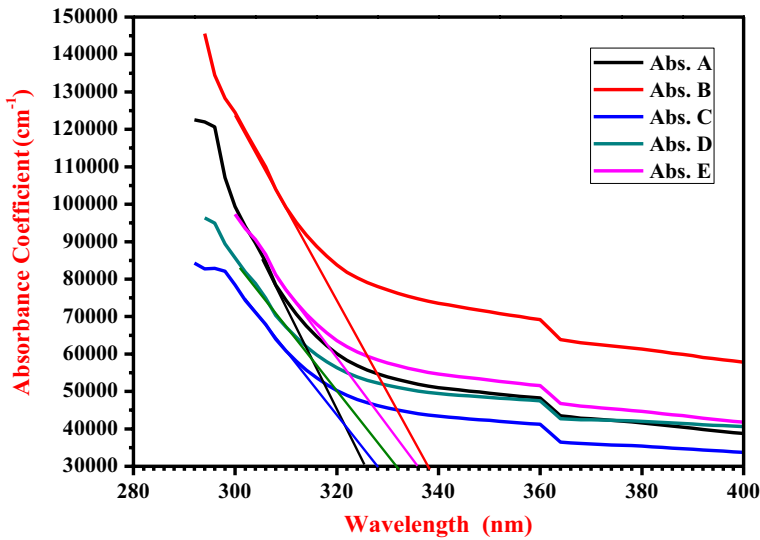


Fig. 6 Absorbance coefficient edge in the nanocomposite shifted with increased CuO ratio

achieved with composition B (1:2/7 wt.%), whereas the lowest value is observed for composition C (1.5:1.5/7 wt.%). Thus composition B give the highest absorption compare with the other compositions for the CuO:NiO/C nanocomposite [8]. This shift is prospective behavior, which indicates the increasing ratio of the CuO element in the nanocomposite film and will decrease the optical band gap [50, 52].

Further, the optical density (D_{opt}) is proportional to both the composition and the film thickness of the sample and is dependent on the absorption for the coated layer. D_{opt} of the present CuO:NiO/C nanocomposite thin films can be determined by utilizing the following equation [50]:

$$D_{opt} = \alpha t \tag{2}$$

where α is the absorbance coefficient (cm^{-1}), and t is the film thickness (cm).

Figure 7 interprets the variance of the optical density (D_{opt}) with the photon energy. The optical density is observed to vary with the photon energy, and its behavior is opposite that of the absorbance coefficient: the optical density increases as photon energy increases along the x -axis, and when the content of CuO:NiO in all samples is increased.

Figure 8 shows the variance in the optical density (D_{opt}) with the wavelength. The behavior is similar to that of the absorbance coefficient, where the optical density decreases with increasing wavelength along the x -axis of all samples.

Skin depth of the nanocomposite

The absorption of the nanocomposite inside the thin films for the electromagnetic wave spectrum is dependent on many factors including thickness, the ratio of doping

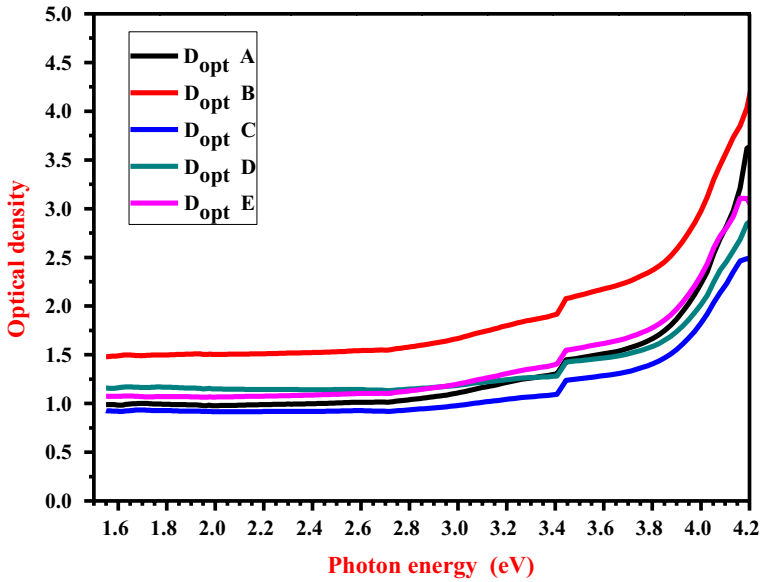


Fig. 7 Variation in optical density of the nanocomposite with photon energy

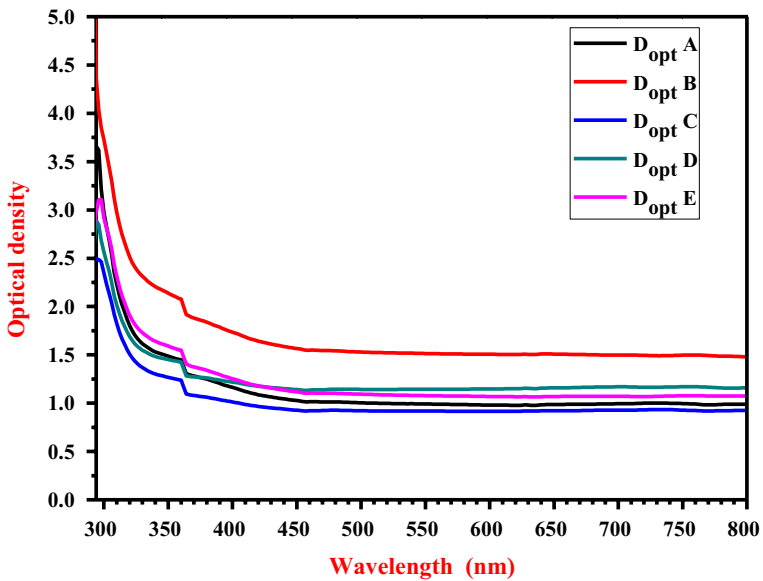


Fig. 8 Variation in optical density of the nanocomposite with the wavelength

material and the extinction coefficient of the thin films. A portion from the incident energy that enters the sample is absorbed as any semiconductor, and the remaining portion of this energy is reflected from the surface. Thus, there are several important factors associated with the photon absorption inside the texture of the thin film, such as skin depth and the optical conductivity of the nanocomposite [7, 8]. Skin depth is also dependent on the photon frequency and the conductivity of the thin films, because the semiconductor conductivity is strongly dependent on the band gap. A correlation between skin depth and optical features is found in any semiconducting material. The skin depth correlates with the absorbance coefficient (α) by the following equation [53]:

$$x = \frac{\lambda}{2\pi k} \tag{3}$$

where x is the skin depth (nm), λ is the wavelength (nm) and κ is the extinction coefficient.

The skin depth can be calculated for the nanocomposite thin films by utilizing the wavelength with extinction coefficient data. Figure 9 shows the dependence of skin depth on the photon energy for the CuO:NiO/C nanocomposite thin films. It is evident from Fig. 9 that the skin depth (x) is increased with increased photon energy and is dependent on the composition of the CuO:NiO in the dopant carbon. The skin depth value decreases with increased photon energy until it becomes zero. When the content of CuO:NiO increases, the skin depth decreases, and the increase in CuO:NiO leads to darkness of the nanocomposite thin films, which reduces the transparency of the thin films. The curves obtained from the skin depth-photon

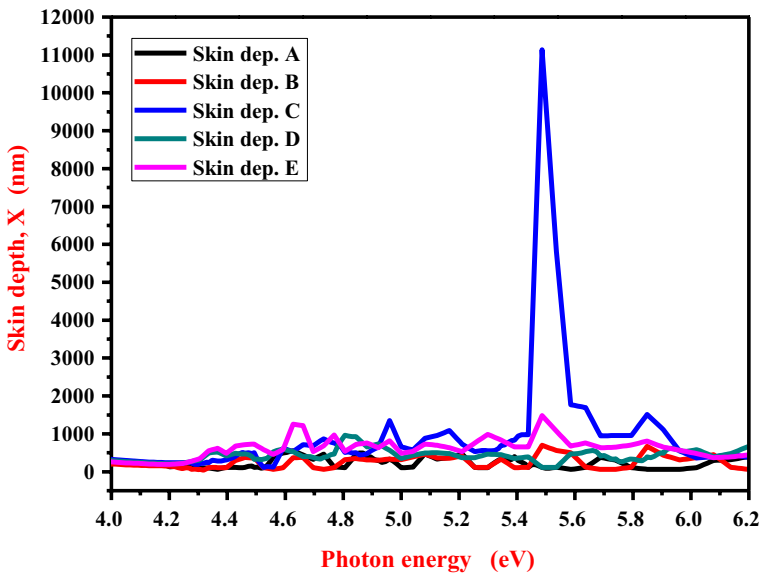


Fig. 9 Skin depth variation with photon energy for the nanocomposite

energy data show a peak value in one region of the photon energy, with the value reaching 5.5 eV.

The peak in Fig. 9 is dependent on the CuO:NiO content in the nanocomposite films. The amplitude of this peak decreases when CuO:NiO content is increased. The skin depth peak found in composition C has an equal amount of CuO and NiO, and exhibits the largest peak, at 5.5 eV value [51, 53].

Transmittance and reflectance for the nanocomposite

Figure 10 shows the optical transmission spectra of carbon (C) thin films with various composition of nano CuO:NiO. The transmittance intensity increases with increasing wavelength. The transmittance is increased when the doped nanomaterial composition of CuO:NiO increases.

The transmittance is invariant along the horizontal axis when the wavelength increases. Figure 10 shows that the transmittance begins at the lower value at the UV region and increases with increasing wavelength up to the visible region ($\lambda = 460$ nm), after which it remains steady along the wavelength axis for all compositions. Also, the transmittance increases with a decrease in the composition of CuO in various compositions only up to a wavelength of ($\lambda = 460$ nm), after which it remains steady. The composition of sample E (2.5:0.5/7 wt.%) is the best content for the CuO:NiO/C nanocomposite and has a lower transmittance value [50, 53].

The optical reflectance spectra of the nanocomposite thin films with various CuO:NiO composition are shown in Fig. 11, which demonstrates that for all compositions, the reflectance decreases with increasing wavelength for samples A, B, C and D, while it increases with increasing wavelength for sample E.

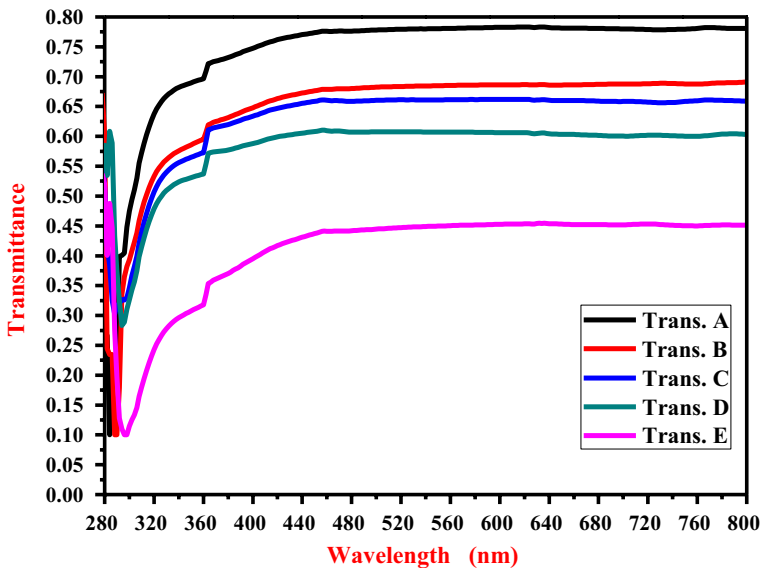


Fig. 10 Transmittance with wavelength for all samples

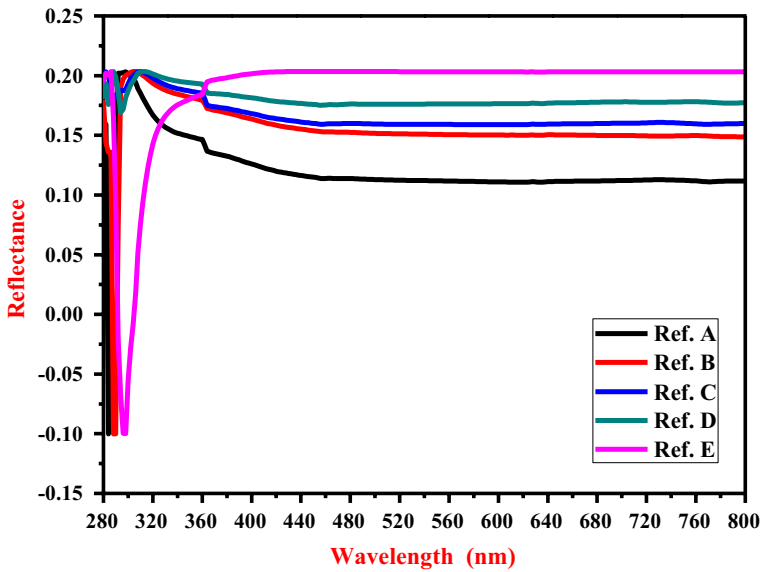


Fig. 11 Reflectance spectra with wavelength for all samples

From these data, the optical absorption for the samples is increased when the reflectance and transmittance values are lower. The surfaces of the deposited thin films for the nanocomposite film on the substrates has a rough nature to harness the incident light in the visible and near-IR regions. This confirms that the incident light over the nanocomposite films is thoroughly absorbed. Therefore, the absorptivity (α) can be computed from the relation between the reflectivity (R) and the absorptivity (α) for all nanocomposite samples, with values of absorptivity (α) of 88–98% [53].

Extinction coefficient and refractive index

A basic optical feature of nanocomposite materials is the refractive index (n), which correlates directly with their optical features [50]. The refractive index was computed from the values of the reflectance and extinction coefficient of the nanocomposite thin films by utilizing the equation:

$$n = \left[\frac{1 + R}{1 - R} \right] + \sqrt{\frac{4R}{(1 - R)^2} - k^2} \tag{4}$$

where n is the refractive index, R is the reflectivity and k is the extinction coefficient.

The analyzed domain of wavelengths for the refractive index to the doped nanocomposite films as shown in Fig. 12. All compositions for the samples are indicating that the refractive index decreases with increasing wavelength for samples (A, B, C, and D) but in the sample (E) increases with wavelength. Then the refractive index is invariant with the wavelength increases along the x -axis.

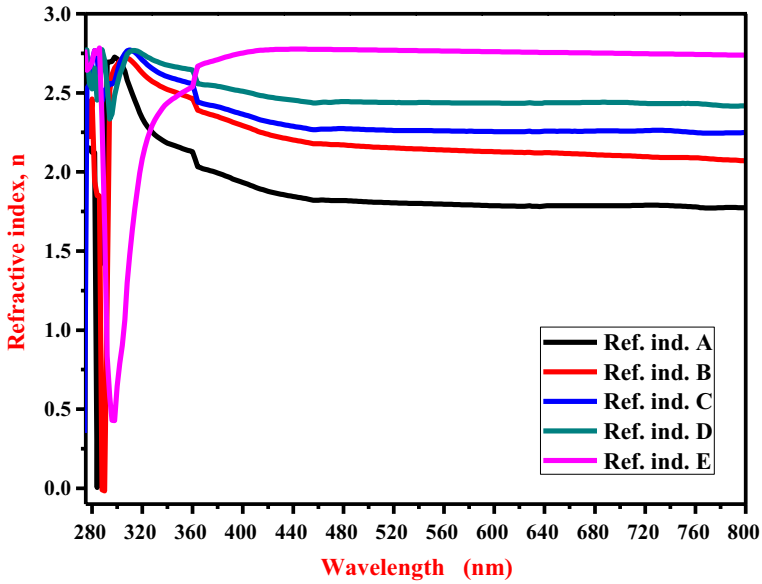


Fig. 12 Refractive index with the wavelength for the nanocomposite

The refractive index demeanor in Fig. 12 was attributed to an increase in nanomaterial content (CuO:NiO) in the nanocomposite was led to increase of the packaging bulk as a result of filler amount for thin films.

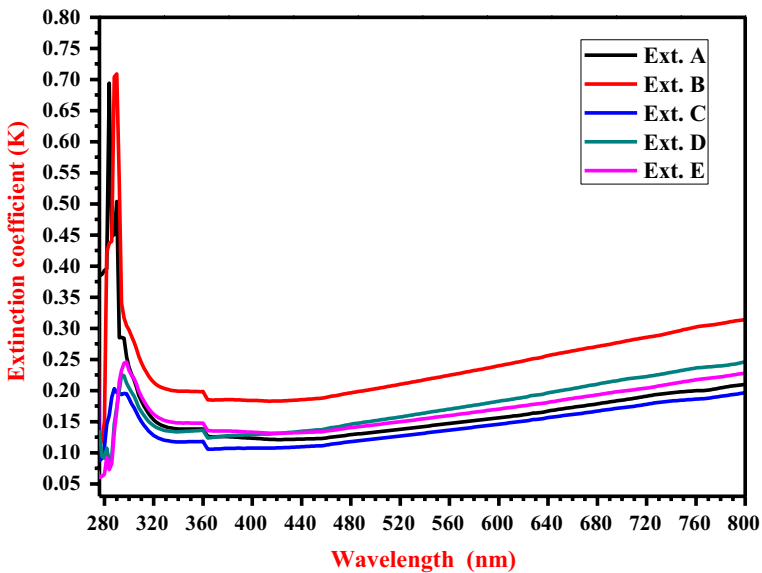


Fig. 13 Extinction coefficient with wavelength for all samples

The extinction coefficient (k) is dependent on the wavelength range for the doped samples of the nanocomposite as shown in Fig. 13. The extinction coefficient for the nanocomposite film shows a decrease in value for wavelengths of 280–360 nm, while it increases for all samples in the wavelength range of 360–800 nm [36].

The extinction coefficient is dependent on the wavelength and the absorption coefficient, and may be calculated by the equation [54, 55]:

$$k = \frac{\alpha \lambda}{4\pi} \quad (5)$$

where α is the absorbance coefficient (cm^{-1}) and λ is the wavelength (cm).

The extinction coefficient increased for nanocomposite thin films with doping composition because of the increase in absorption coefficient and wavelength. Figure 13 demonstrates that the extinction coefficient decreases to a lower value at a wavelength range of 300–360 nm and then increases at a wavelength range of 360–800 nm, which is due to the doping process for the carbon with nano CuO:NiO.

Real and imaginary of dielectric constant

The dielectric constant of the nanocomposite thin films has two parameters: real (ϵ_1) and imaginary (ϵ_2) parts. This relationship can be expressed as $(\omega) = \epsilon_1(\omega) + i\epsilon_2(\omega)$. These parameters depend on n and k values, and are therefore computed from the equations [51, 56]:

$$\begin{cases} \epsilon_1 = n^2 - k^2 \\ \epsilon_2 = 2nk \end{cases} \quad (6)$$

where the values of (ϵ_1) and (ϵ_2) are dependent on the wavelength, n and k parameters.

The real (ϵ_1) and imaginary (ϵ_2) merit is increased with increasing wavelength and with carbon doping of the CuO:NiO nanomaterials, as shown in Figs. 14 and 15, which demonstrate the values of these parameters for the dielectric constant. In Fig. 14, the real part (ϵ_1) is related to the values of the refractive index (n) and the extinction coefficient (k) with Eq. (6). Therefore, n is higher than k , and the figure will be of the same shape as the refractive index (n) [50, 56].

In Fig. 15, the imaginary part (ϵ_2) of the dielectric constant is also related to n and k , but the value of k is lower than that of n , and when multiplying k by n , the result is low, and the shape of Fig. 15 is the same as the figure of the extinction coefficient.

Optical conductivity for the nanocomposite

The optical conductivity (σ) was correlated to the absorbance coefficient (α) and the refractive index (n) and is computed by utilizing this equation [57]:

$$\sigma = \frac{\alpha n c}{4\pi} \quad (7)$$

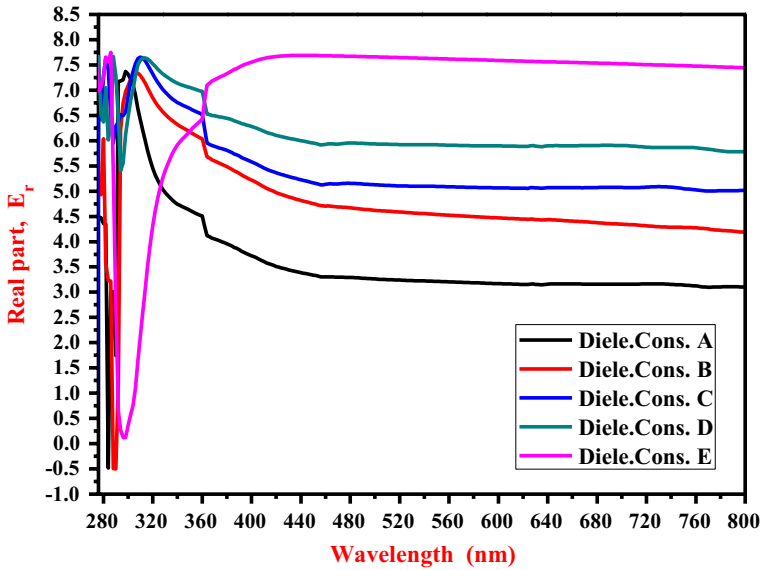


Fig. 14 Real part of dielectric constant with wavelength for all samples

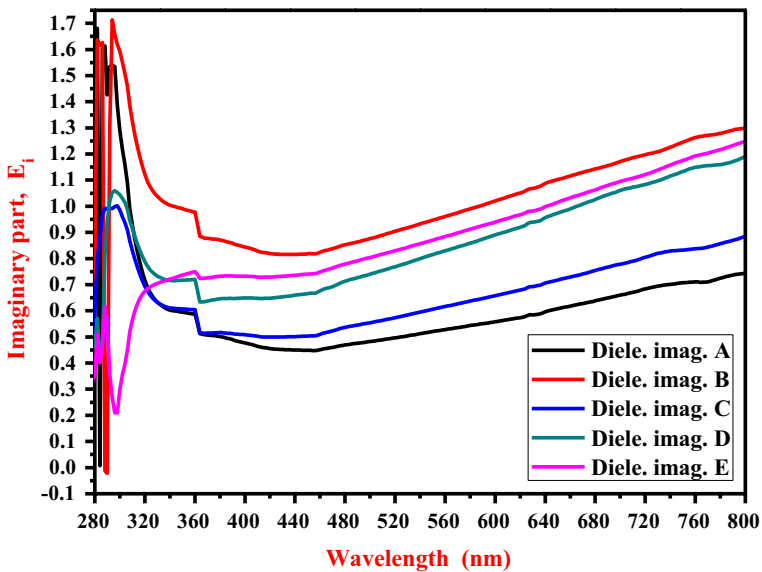


Fig. 15 Imaginary part of dielectric constant with wavelength for all samples

where σ is the optical conductivity ($\Omega \cdot \text{cm}^{-1}$), α is the absorbance coefficient (cm^{-1}) and (n) is the refractive index, and (c) is the velocity of light (3×10^{10} cm/s).

Figure 16 demonstrates the variance between optical conductivity and wavelength. As can be seen, the optical conductivity has high value at a wavelength of

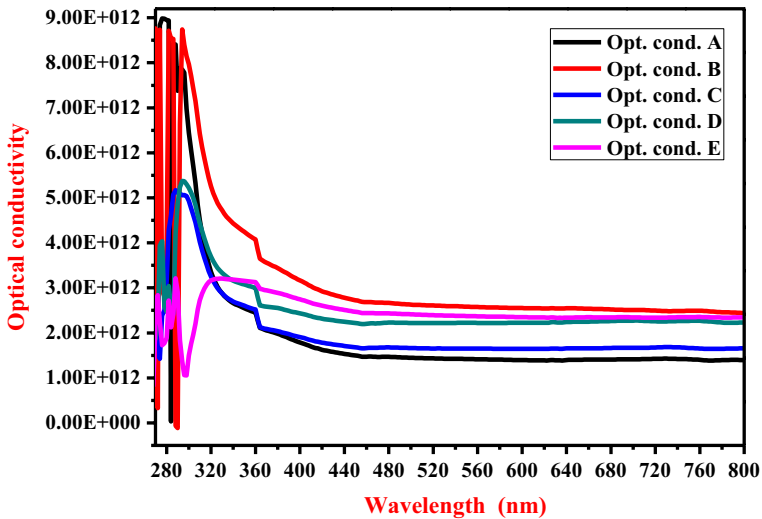


Fig. 16 Optical conductivity with wavelength for all samples

320 nm, and decreases along the *x*-axis of the wavelength with an increase in the doping nanomaterials of CuO:NiO to carbon (C). The composition *B* has high optical conductivity from the other amount of composition as shown in Fig. 16 [7].

Optical energy gap for the nanocomposite

The nanocomposite band gap is defined by utilizing Tauc’s relation and is dependent on the absorption coefficient (α) and the photon energy ($h\nu$), as shown in the following equation:

$$ah\nu = A(h\nu - E_g)^n \tag{8}$$

where *A* is a constant, E_g is the energy gap of the nanocomposite, and *n* is the power representing the value of the allowed transition ($n=0.5$ for indirect transition and $n=2$ for direct transition) [58]. The high absorption energy of the electron in the nanocomposite in the confined region of the energy gap between the valence band and the conduction band causes acceleration of the electrons to move between bands. This depends on the absorption wavelength of each composition for the nanocomposite thin films.

Practically, to locate the energy gap of the CuO:NiO/C nanocomposite thin films, the photon energy ($h\nu$) vs. $(ah\nu)^2$ is plotted utilizing the information obtained from the optical absorption spectra, as demonstrated in Fig. 17 [36, 51].

The plot obtained shows a direct line in a definite region. Therefore, to obtain the direct allowed transition of the energy gap (E_g) of the nanocomposite thin films dependent on the CuO:NiO composition, the direct line is extended and it is intersected at ($h\nu$) in the X-axis. It can be observed that the optical energy

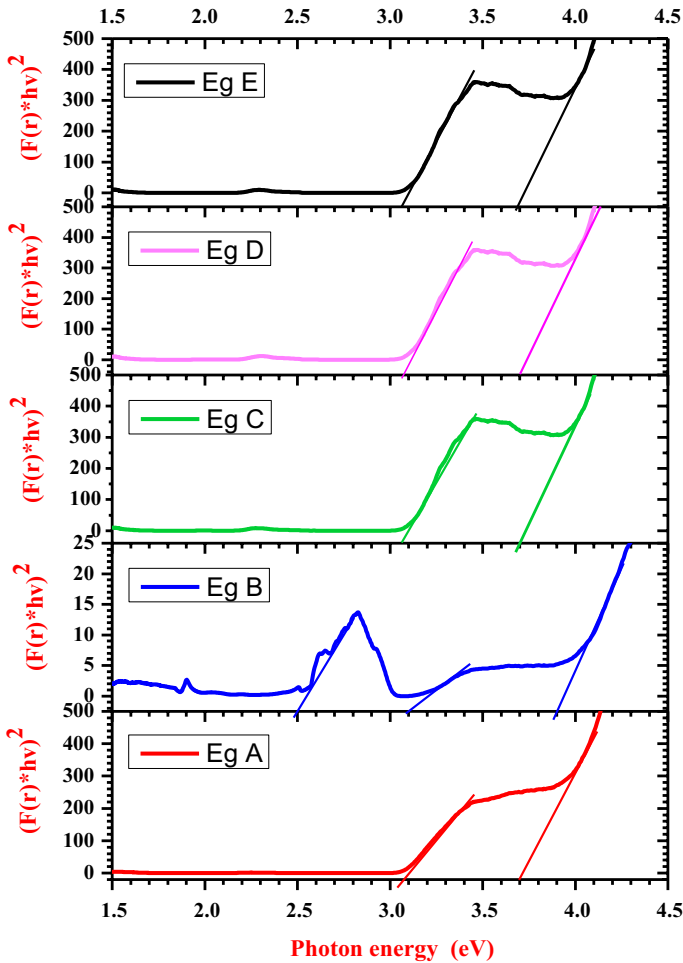


Fig. 17 Energy gap for all nanocomposite thin films

gap decreases with increasing CuO content in the nanocomposite films [8, 58]. The value of the energy gap ranges from 2.5 to 3.9 eV; composition A, C, D and E have the same energy gap (3.1 and 3.7 eV) which is dependent on the CuO and NiO in the nanocomposite to dope carbon (C), but composition B has three energy gap values (2.5, 3.1 and 3.9), as shown in Fig. 17. The reason for this is because the amount of NiO to dope carbon was 2.5 and CuO was 1 wt.%, which led to this behavior, as the content of NiO was higher than CuO. Thus the behavior of composition B is irregular, which is due to the mixing of the mixture or the precipitation of the composition over the glass substrate [50, 53].

Absorption band tail (Urbach energy)

Semiconductor materials that have optical absorption spectra play an important role because they provide the principal data about the contents and band gap. The optical absorbance spectra of a semiconductor may be classified into two essential parts: (1) a region of weak absorbance, which can appear because of impurities, defects, or disordered lattice structure for the nanocomposite, (2) high absorbance, which is determined from the optical energy gap. The Urbach band tail is an exponential part that may be near the band gap edge and along the absorbance coefficient curvature; the exponential band tail shows poor crystallinity, and materials have an amorphous and disordered structure. The Urbach practical base takes place in the lowest field of photon energy, by depending on the absorbance coefficient (α) and photon energy ($h\nu$), which is known by the equation [48, 50]:

$$\alpha = \alpha_o \exp \frac{h\nu}{E_u} \quad (9)$$

where α_o is a constant, and E_U is the Urbach energy.

Taking the logarithms for the two sides of Eq. (9) gives a straight line equation and becomes:

$$\ln \alpha = \ln \alpha_o + \frac{h\nu}{E_u} \quad (10)$$

Theoretically, the Urbach energy (E_U) may be obtained from the slope of the straight line by plotting $\ln(\alpha)$ versus the photon energy ($h\nu$) on a horizontal axis. Figure 18 shows a graphic representation of $\ln(\alpha)$ against ($h\nu$). The slope for a straight line is equal to ($1/E_U$) and by intersecting the y -axis in an amount is equal to $\ln(\alpha_o)$ for the nanocomposite thin films [50].

It may be observed that the value of the Urbach energy (E_U) is increased by increasing the rate of the CuO:NiO amount in the nanocomposite films, but the correlation is exactly linear by taking a suitable fitting of all curves [50]. Further, it may be observed from Fig. 18 that the relation for the Urbach energy (E_u) and the photon energy ($h\nu$) will be fitted to obtain a linear interrelation for all composition of the nanocomposite thin films.

The results for the paper can be summarized in Table 2.

Conclusion

Spun nanocomposite thin films of CuO:NiO/C for various rates ($0.5:2.5 \leq x \leq 2.5:0.5$) wt.%, were deposited on preheated copper (Cu) and glass substrates. Optical analysis revealed that the nanocomposite thin films have good crystalline surface morphology, and exhibited a shift in the optical absorption edge to higher wavelengths with the addition of carbon doping to CuO:NiO. The

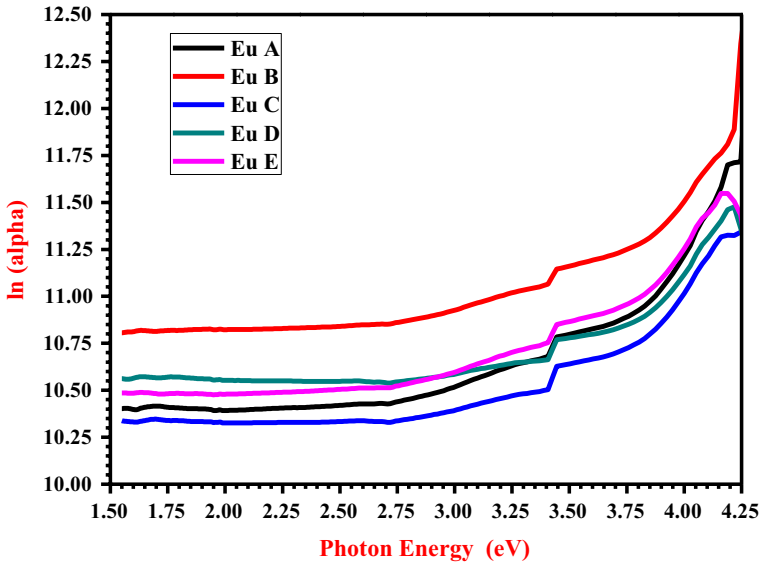


Fig. 18 Urbach energy with photon energy for all samples

Table 2 Results of the absorbance edge, energy gap (E_g), Urbach energy (E_u) and (α_o) constant for the nanocomposite thin films

Nanocomposite thin film (wt %)	Absorbance edge (nm)	Energy gap (E_g) (nm)	Urbach energy (E_u) (nm)	(α_o) constant* 10^3 (cm^{-1})
A (0.5:2.5/7)	326	3.1, 3.7	2.86	15.99
B (1:2/7)	338	2.5, 3.1, 3.9	4.76	32.86
C (1.5:1.5/7)	328	3.1, 3.7	37.04	30.64
D (2:1/7)	332	3.1, 3.7	11.91	32.86
E (2.5:0.5/7)	336	3.1, 3.7	47.62	36.32

high absorbance obtained by doping is important for use of the nanocomposite as a coating on a flat plate collector to absorb solar energy. For these nanocomposite film samples, a higher absorption coefficient (α) was determined. The skin depth (x) and optical density (D_{opt}) were computed and discussed. The energy band gap results were calculated, and the values ranged from 3.9 to 2.5 eV. Carbon was doped with a certain amount of nanomaterials (CuO:NiO), and the values of the energy gap were determined, revealing that the energy gap values were decreased, which compared favorably with results reported by other researchers. The Urbach energy (E_u) and its components were determined for the nanocomposite, and it was found to be dependent on the absorbance coefficient for the nanocomposite.

From these results it was ascertained that the nanocomposite thin films are a semiconductor.

The TEM examination, conductivity, I – V characteristics, chemistry concept, band gap and quantum yield of the CuO–NiO/C composite will be taken into consideration for future work.

Acknowledgments This work was supported by Al-Nahrain University (Grant No. 64074), Department of Chemistry, College of Science and Department of Mechanical Engineering, Engineering College.

References


- Liu YK, Zapfen JA, Shan YY, Geng CY, Lee CS, Lee ST (2005) Wavelength-controlled lasing in $Zn_xCd_{1-x}S$ single-crystal nanoribbons. *Adv Mater* 17:1372–1377
- Rani TD, Tamilarasan K, Elangovan E, Leela S, Ramamurthi K, Thangaraj K, Himcinschi C, Trenkmann I, Schulze S, Hietschold M, Liebig A, Salvan G, Zahn DRT (2015) Structural and optical studies on Nd doped ZnO thin films. *Superlattices Microstruct* 77:325–332
- Ali M, Syed WAA, Zubair M, Shah NA, Mehmood A (2013) Physical properties of Sb-doped CdSe thin films by thermal evaporation method. *Appl Surf Sci* 284:482–488
- Khomane AS (2013) Crystallographic and microscopic properties of ternary $CdS_{0.5}Se_{0.5}$ thin films. *J Optics* 124:2432–2435
- Pan AL, Yang H, Liu RB, Yu RC, Zou BS, Wang ZL (2005) Color-tunable photoluminescence of alloyed CdS_xSe_{1-x} nanobelts. *J Am Chem Soc* 127:15692–15693
- Pulker HK (1999) *Coatings on Glass*. 2nd edn, p 343
- Kumar S, Bukkigar SD, Singh S, Pratibha V, Singh KR, Reddy NP, Shetti ChV, Reddy V, Sadhu S Naveen (2019) Electrochemical sensors and biosensors based on graphene functionalized with metal oxide nanostructures for healthcare applications. *Chem Sel* 4:5322–5337
- Hassanien AS, Akl AA (2015) Influence of composition on optical and dispersion parameters of thermally evaporated non-crystalline $Cd_{50}S_{50-x}Se_x$ thin films. *J Alloy Compd* 648:280–290
- Gutierrez MT, Ortega J (1989) Electrochemical preparation and characterization of n-CdSe_{0.65}Te_{0.35} polycrystalline thin films: influence of annealing. *Sol Energy Mater* 19:383–393
- Gutierrez MT, Ortega J (1990) Influence of chemical and photoelectrochemical etching on the n-CdSe_{0.65}Te_{0.35} polycrystalline thin films: application in the PEC cells. *Sol Energy Mater* 15:387–394
- Mirovsky Y, Tenne R, Hodes G, Cahen D (1982) Photoelectrochemical solar cells: interpretation of cell performance using electrochemical determination of photoelectrode properties. *Thin Solid Films* 91:349–356
- Maia FF Jr, Freire JAK, Freire VN, Farias GA, da Silva EF (2004) Interface properties in ZnSe/ZnS based strained superlattices and quantum wells. *Appl Surf Sci* 237:261–265
- Choudhari JB, Deshpande NG, Gudage YG, Ghosh A, Huse VB, Sharma R (2008) Studies on growth and characterization of ternary $CdS_{1-x}Se_x$ alloy thin films deposited by chemical bath deposition technique. *Appl Surf Sci* 254:6810–6816
- Shahane GS, More BM, Rotti CB, Deshmukh LP (1997) Studies on chemically deposited $CdS_{1-x}Se_x$ mixed thin films. *Mater Chem Phys* 47:263–267
- Yadav AA, Masumdar EU (2010) Optical and electrical transport properties of spray deposited $CdS_{1-x}Se_x$ thin films. *J Alloy Compd* 505:787–792
- Mane RS, Lokhande CD, Todkar VV, Chung H, Yoon MY, Han SH (2007) Photosensitization of nanocrystalline TiO₂ film electrode with cadmium sulphoselenide. *Appl Surf Sci* 253:3922–3926
- Tranquada JM (1997) Modulated spin and charge densities in cuprate superconductors. *Phys B* 241–243:745–750
- Balakirev FF, Betts JB, Migliori A, Ono S, Ando Y, Boebinger GS (2003) signature of optimal doping in Hall-effect measurements on a high-temperature superconductor. *Nature* 424:912–915
- Habibi MH, Karimi B, Zendehelel M, Habibi M (2003) Fabrication, characterization of two nanocomposite CuO–ZnO working electrodes for dye sensitized solar cell. *Spectrochim Acta Part A Mol Bio-mol Spectrosc* 116:374–380

20. Cao F, Wang T, Ji X (2019) Enhanced Visible Photocatalytic Activity of Tree-like ZnO/CuO Nanostructure on Cu Foam. *Appl Surf Sci* 471:417–424
21. Joseph A, Mohan S, Sujith Kumar CS, Mathew A, Thomas S, Vishnu BR, Sivapirakasam SP (2019) An experimental investigation on pool boiling heat transfer enhancement using sol-gel derived nano-CuO porous coating. *Exp Therm Fluid Sci* 103:37–50
22. Zhuang S, Lu M, Zhou N, Zhou L, Lin D, Peng Z, Wu Q (2019) Cu modified ZnO nanoflowers as photoanode material for highly efficient dye sensitized solar cells. *Electrochim Acta* 294:28–37
23. Salaria H, Sadeghinia M (2019) MOF-templated synthesis of nano Ag₂O/ZnO/CuO heterostructure for photocatalysis. *J Photochem Photobiol A* 376:279–287
24. Naji IS (2019) Characterization of CuO-doped tin dioxide thin films prepared by pulsed-laser deposition for gas-sensing applications. *J Nanomater Nanoeng Nanosyst* 233:17–25
25. Prasanth D, Sibin KP, Barshilia HC (2019) Optical properties of sputter deposited nanocrystalline CuO thin films. *Thin Solid Films* 673:78–85
26. Said AAA, Abd El-Wahab MM, Soliman SA, Goda MN (2014) Synthesis and characterization of nano CuO–NiO mixed oxides. *Nanosci Nanoeng* 2:17–28
27. Tawfik WZ, Khalifa ZS, Abdel-wahab MSh, Hammad AH (2019) Sputtered cobalt doped CuO nano-structured thin films for photoconductive sensors. *J Mater Sci Mater Electron* 30:1275–1281
28. Adler D, Feinle J (1970) Electrical and optical properties of narrow-band materials. *Phys Rev B* 2(2):3112–3134
29. Manimenaka S, Umadevi G, Manickam M (2017) Effect of copper concentration on the physical properties of copper doped NiO thin films deposited by Spray pyrolysis. *Mater Chem Phys* 191:181–187
30. Haider AJ, Al-Anbari R, Sami HM, Haider MJ (2019) Photocatalytic Activity of Nickel Oxide. *J Mater Res Technol* 8:2802–2808
31. Al-Ghamdi AA, Mahmouda WE, Yaghmour SJ, Al-Marzouki FM (2009) Structure and optical properties of nanocrystalline NiO thin film synthesized by sol-gel spin-coating method. *J Alloy Compd* 486:9–13
32. Al-Sehemi AG, Al-Shihri AS, Kalam A, Du G, Ahmad T (2014) Microwave synthesis, optical properties and surface area studies of NiO Nanoparticles. *J Mol Struct* 1058:56–61
33. Dolai S, Sarangi SN, Hussain S, Bhar R, Pal AK (2019) Magnetic properties of nanocrystalline nickel incorporated CuO thin films. *J Magn Magn Mater* 479:59–66
34. Zhang J, Hao B, Zhang X, Yuan H, Zhang Z, Yang L (2019) The influence of microstructure and emissivity of NiO-doped Fe₃O₄ spinel structure on near- and middle-infrared radiation. In: *Characterization of minerals, metals, and materials, conference proceedings*, pp 69–77
35. Achary AD, Sharma P, Sharma D, Poonia P, Sarwan B, Dwivedi HK (2019) Preparation and characterization of PVA-NiO Composite. In: *AIP conference proceedings*, vol 2100, pp 1–4
36. Achary AD, Sarwan B, Malik IA, Bhat YA, Silwa K, Rathore MK (2019) Optical properties of NiO:PVA thin films. In: *AIP conference proceedings* vol 2100 pp 1–5
37. Reddy KR, Reddy ChV, Nadagouda MN, Shetti NP, Jaesool S, Aminabhavi TM (2019) Polymeric graphitic carbon nitride (g-C₃N₄)-based semiconducting nanostructured materials: synthesis methods, properties and photocatalytic applications. *J Environ Manage* 238:25–40
38. Reddy KR, Sin BCh, Ho Yoo Ch, Park W, Ryu KS, Lee JS, Sohnc D, Lee Y (2008) A new one-step synthesis method for coating multi-walled carbon nanotubes with cuprous oxide nanoparticles. *Scripta Mater* 58:1010–1013
39. Haque E, Kim J, Malgras V, Reddy KR, Ward AC, You J, Bando Y, Hossain MdShA, Yamauchi Y (2018) Recent advances in graphene quantum dots: synthesis, properties, and applications. *Small Methods* 2(1800050):1–14
40. Mehta A, Mishra A, Basu S, Shetti NP, Reddy KR, Saleh TA, Aminabhavi TM (2019) Band gap tuning and surface modification of carbon dots for sustainable environmental remediation and photocatalytic hydrogen production—A review. *J Environ Manage* 250(109486):1–15
41. Cakici M, Reddy KR, Marroquin FA (2017) Advanced electrochemical energy storage supercapacitors based on the flexible carbon fiber fabric-coated with uniform coral-like MnO₂ structured electrodes. *Chem Eng J* 309(2017):151–158
42. Reddy NL, Rao VN, Vijayakumar M, Santhosh R, Anandan S, Karthik M, Shankar MV, Reddy KR, Shetti NP, Nadagouda MN, Aminabhavi TM (2019) A review on frontiers in plasmonic nano-photocatalysts for hydrogen production. *Int J Hydrogen Energy* 44:10453–10472

43. Reddy KR, Sin BCh, Ryu KS, Noh J, Lee Youngil (2009) In situ self-organization of carbon black–polyaniline composites from nanospheres to nanorods: synthesis, morphology, structure and electrical conductivity. *Synth Met* 159:1934–1939
44. Dakshayini BS, Reddy KR, Mishra A, Shetti NP, Malode SJ, Basu S, Naveen S, Raghu AV (2019) Role of conducting polymer and metal oxide-based hybrids for applications in amperometric sensors and biosensors. *Microchem J* 147:7–24
45. Haque E, Yamauchi Y, Malgras V, Reddy KR, Yi JW, Hossain MdShA, Kim J (2018) Nanoarchitected graphene-organic frameworks (GOFs): synthetic strategies, properties, and applications. *Chem Asian J* 13:1–15
46. Mishra A, Mehta A, Basu S, Shetti NP, Reddy KR, Aminabhavi TM (2019) Graphitic carbon nitride ($g-C_3N_4$)-based metal-free photocatalysts for water splitting: a review. *Carbon* 149:693–721
47. Shetti NP, Malode ShJ, Nayak DS, Aminabhavi TM, Reddy KR (2019) Nanostructured silver doped $TiO_2/CNTs$ hybrid as an efficient electrochemical sensor for detection of anti-inflammatory drug, cetirizine. *Microchem J* 150(104124):1–8
48. Urbach F (1953) The long-wavelength edge of photographic sensitivity and of the electronic absorption of solids. *Phys Rev J Arch* 92:1324
49. El-Hagary M, Ismail ME, Shaaban ER, El-Taher A (2012) Effect of γ -irradiation exposure on optical properties of chalcogenide glasses $Se_{70}S_{30-x}Sb_x$ thin films. *Radiat Phys Chem* 81:1572–1577
50. Al-Taa'y W, Nabi MA, Yusop RM, Yousif E, Abdullah BM, Salimon J, Salih N, Zubairi SI (2014) Effect of nano ZnO on the optical properties of poly(vinyl chloride) Films. *Int J Polym Sci* 2014(697809):1–6
51. Al-Taa'y WA, Ameer AA, Al-Dahhan WH, Abdallh M, Yousif E (2015) Optical constants of poly(vinyl chloride) doped by nano ZnO. *J Chem Pharm Res* 7:536–541
52. Sanchez-Ramirez EA, Hernandez-Perez MA, Aguilar-Hernandez J, Rangel-Salinas E (2014) Nanocrystalline $CdS_{1-x}Se_x$ alloys as thin films prepared by chemical bath deposition: effect of x on the structural and optical properties. *J. Alloys Compd* 615:S511–S514
53. Al-Taa'y WA, Oboudi SF, Yousif E, Nabi MA, Yusop RM, Derawi D (2015) Fabrication and characterization of nickel chloride doped PMMA films. *Adv Mater Sci Eng* 2015(913260):1–5
54. P. Obreja, M. Kusko, D. Cristea, M. Puric, F. Comanescu (2010) influence of $AlCl_3$ on the optical properties of new synthesized 3-armed poly (methyl methacrylate) films. In: Proceedings of the symposium on photonics technologies for 7th frame work program, pp. 392–395, Wroclaw
55. Abdullah OG, Saber DR (2012) Optical absorption of poly-vinyl alcohol films doped with nickel chloride. *Appl Mech Mater* 110–116:177–182
56. Pankove JI (1975) Optical processes in semiconductors. Dover, New York
57. Xiang J, Lu W, Hu Y, Wu Y, Yan H, Lieber CM (2006) Ge/Si nanowire heterostructures as high-performance field-effect transistors. *Nature* 441:489–493
58. Sanchez-Ramirez EA, Hernandez-Perez MA, Aguilar-Hernandez JR (2015) Study on the introduction of Se into CdS thin films: influence on the kinetics of the deposition and the structural and optical properties. *Appl Surf Sci* 347:35–39

Publisher's Note Springer Nature remains neutral with regard to jurisdictional claims in published maps and institutional affiliations.

Affiliations

Rasheed N. Abed¹  · Mustafa Abdallh² · Alaa A. Rashad² · Abas Hadaway³ · Emad Yousif²

¹ Mechanical Engineering Department, Engineering College, Al-Nahrain University, Baghdad, Iraq

² Department of Chemistry, College of Science, Al-Nahrain University, Baghdad, Iraq

³ School of Engineering, London South Bank University, 103 Borough Road, London SE1 0AA, UK